RESEARCH ARTICLE | JUNE 28 2022

SnO_2 modified mesoporous ZrO_2 as efficient electron-transport layer for carbon-electrode based, low-temperature mesoscopic perovskite solar cells

De'en Guo; Jiao Ma; Siyuan Lin; Xiao Guo; Han Huang ; Deming Kong; Fuxin Xu; Yongli Gao ; Wenhao Zhang; Yue Hu ; Conghua Zhou

Appl. Phys. Lett. 120, 263502 (2022)
https://doi.org/10.1063/5.0087943
CHORUS

Applied Physics Letters ARTICLE scitation.org/journal/apl

SnO_2 modified mesoporous ZrO_2 as efficient electron-transport layer for carbon-electrode based, low-temperature mesoscopic perovskite solar cells

Cite as: Appl. Phys. Lett. **120**, 263502 (2022); doi: 10.1063/5.0087943
Submitted: 11 February 2022 · Accepted: 12 June 2022 ·
Published Online: 28 June 2022

De'en Guo,[1] Jiao Ma,[1] Siyuan Lin,[1] Xiao Guo,[1] Han Huang,[1] Deming Kong,[1] Fuxin Xu,[1] Yongli Gao,[2] Wenhao Zhang,[3] Yue Hu,[3] and Conghua Zhou[1,a)]

AFFILIATIONS

[1]Hunan Key Laboratory of Super-microstructure and Ultrafast Process, Hunan Key Laboratory of Nanophotonics and Devices, School of Physics and Electronics, Central South University, Changsha, Hunan 410083, China
[2]Department of Physics and Astronomy, University of Rochester, Rochester, New York 14627, USA
[3]Michael Grätzel Center for Mesoscopic Solar Cells, Wuhan National Laboratory for Optoelectronics, Huazhong University of Science and Technology, Wuhan 430074, People's Republic of China

[a)]Author to whom correspondence should be addressed: chzhou@csu.edu.cn

ABSTRACT

SnO_2 modified mesoporous ZrO_2 is used to replace the mesoporous TiO_2 layer and serves as a kind of mesoporous electron-transport layer during the low-temperature fabrication of mesoscopic perovskite solar cells that are based on carbon electrode. X-ray/ultraviolet photoelectron spectroscopy studies and electrical test observe that SnO_2 modification brought down the work function while increasing the conductivity of the mesoporous ZrO_2. Transient photovoltage/photocurrent decay curves, impedance spectroscopy, and photoluminescence mapping show that after the bottom layer of ZrO_2 is modified by SnO_2, the charge extraction process is accelerated while recombination is retarded. This modification helps to increase the power conversion efficiency from 4.70 (±0.85)% to 10.15 (±0.35)%, along with the optimized efficiency at 13.37% (AM1.5G, 100 mW/cm^2) for the low-temperature devices. In addition, the effects of modification layers of SnO_2 on the power conversion properties are carefully studied. This study shows that SnO_2 modified mesoporous ZrO_2 could serve as an efficient electron-transport layer for the low-temperature mesoscopic devices.

Organic–inorganic hybrid perovskite solar cells (PSCs) have developed very fast since the pioneered work of Miyasaka *et al.*[1] The power conversion efficiency (PCE) has increased from 3.8% (AM1.5G, 100 mW cm^{-2}) to the recorded 25.7%,[1–5] owing to the optimization on light-absorbing material,[6] charge-transport material,[7] device structure,[8] and so on. Stability and cost are suggested to be the main bottlenecks for the practical mass application. Carbon materials are known by the high electrical conductivity and low price. Moreover, carbon electrode owns a work function near 5.0 eV and sound corrosion resistance. As such, PSCs based on carbon electrode (noting as CPSCs) have also developed quickly, and several structures have been proposed, including mesoscopic (meso CPSCs),[9–12] embedment,[13,14] quasi-planar,[15] and planar structures.[16,17] In 2021, Xiao *et al.* applied acetamidine mixed perovskite to prepare the photoactive material and achieved PCE higher than 18% in meso CPSCs.[18,19] In 2019, Yang *et al.* modified TiO_2 with $PbTiO_3$ to prepare the electron-transport layer and achieved PCE of 16.37% in the embedment CPSCs.[20] In 2021, Wu and co-workers introduced a simple amphiphilic silane interfacial linkage strategy and achieved a PCE of 18.64% in planar CPSCs.[21] Moreover, prolonged stability has also been demonstrated for the CPSCs. For example, Han's group tested the printable mesoscopic perovskite solar cell that filled with $(5\text{-AVA})_x MA_{1-x}PbI_3$ at 55 °C ± 5 °C for more than 9000 h, but no significant degradation was observed.[22]

Among these carbon-electrode based devices, meso CPSCs are unique for their architecture and air-compatible production procedures. However, they are usually fabricated in high temperatures (400–450 °C), partially due to the need to sinter TiO_2 (to obtain higher conductivity).

This process adds to the production period and the cost. To reduce the cost, low-temperature production is recommended, similar to that done in metal-electrode based PSCs and other types of CPSCs.[23–27] Honestly, in our previous work, low-temperature preparation of meso CPSCs was realized with the architecture of "ITO/SnO_2/meso-TiO_2/meso-ZrO_2/carbon," which was successfully produced in temperatures $\leq$150 °C.[28] However, during that work, TiO_2 was used as the mesoporous electron-transport layer (meso-ETL). Without high temperature (450 °C) sintering, the conductivity of TiO_2 was relatively low, which affected device efficiency. As a result, it is essential to explore a kind of meso-ETL that is compatible with low-temperature procedures. SnO_2 has been shown to be a kind of excellent electron-transport material that could be prepared in low temperatures.[29–32] Here, in this article, SnO_2 is used to modify mesoporous ZrO_2, then replace the meso TiO_2 layer and serve as the meso ETL.

The fabrication process of the low-temperature meso CPSCs is shown in Fig. 1(a). The structure of "FTO/SnO_2/meso-ZrO_2@SnO_2/meso-ZrO_2/carbon" is adopted. For comparison, the device is also prepared using meso TiO_2 as ETL.[28] Details about the preparation procedures are referred to the experimental section shown in the supplementary material. Two points are worthy to note: (i) In order to harvest photo-generated charge carriers, two-layer ETLs are adopted: one is the compact layer and the other is the mesoporous layer. The usage of meso ETL is to increase the contact area between the active layer and the charge-extraction layer. During the past years, meso-TiO_2 was used in most. Herein, such layer is replaced by SnO_2 modified meso-ZrO_2 (or noted by meso-ZrO_2@SnO_2). Such layer is obtained by spin-coating SnO_2 quantum dots (QDs) solution on top of the ZrO_2 blocking layer. To examine the effect of the number of modifying layers on device performance, the number of the modification layers is changed from 0 to 3. After that, two more layers of meso ZrO_2 layers are spin-coated on top to prepare the blocking layer (between the bottom ETL and top carbon electrode). (ii) The carbon electrode is prepared using ZrO_2 inorganic sols, instead of TiO_2 sols.[28] This could avoid the photocatalytic effect brought by TiO_2.[33] Discussion on this topic will be detailed in a forthcoming work. Cross section morphological properties of meso CPSCs are studied by scanning electron microscope (SEM), along with element distribution maps (EDS). Typical cross-section image is shown in Fig. 1(b). Clearly, layered skeleton can be distinguished, such as meso-ZrO_2@SnO_2, meso-ZrO_2, and carbon electrode. After uploading of perovskite crystallites, the three layers are united, which facilitates the power conversion processes.

EDS mapping shows a similar result. Elements of I and Pb distribute throughout the mesoporous layers covering SnO_2, ZrO_2, and carbon electrode, indicating that the perovskite precursor can penetrate to the bottom of the mesoporous skeleton. It is observed that the number of modification layers brings less effect on the distribution of perovskite in the device. Crystallographic characteristics of the devices are studied by x-ray diffraction (XRD), as shown in Fig. S2. Peaks at around 14.23°, 20.13°, 23.61°, 28.30°, 31.75°, 40.56°, and 43.16° can be observed, corresponding to facet planes of (110), (112), (111), (004), (310), (202), and (212) of $(5\text{-AVA})_x(MA)_{1-x}PbI_3$, respectively.[28] No prominent peak is observed for PbI_2, implying that perovskite crystallization could be harvested in the mesoporous skeleton.

Surface chemical properties and work function of the meso-ZrO_2 are characterized by x-ray/ultraviolet photoelectron spectroscopy (XPS/UPS). As shown in Fig. 1(c), before the SnO_2 modification, peaks belong to Zr and O exist. After the modification (one-layer), new peaks at 495.3 and 486.8 eV appear, which belong to $Sn3d_{3/2}$ and $Sn3d_{5/2}$, respectively, implying SnO_2QDs have been mounted on ZrO_2. According to the UPS study [Fig. 1(d)], the work function of

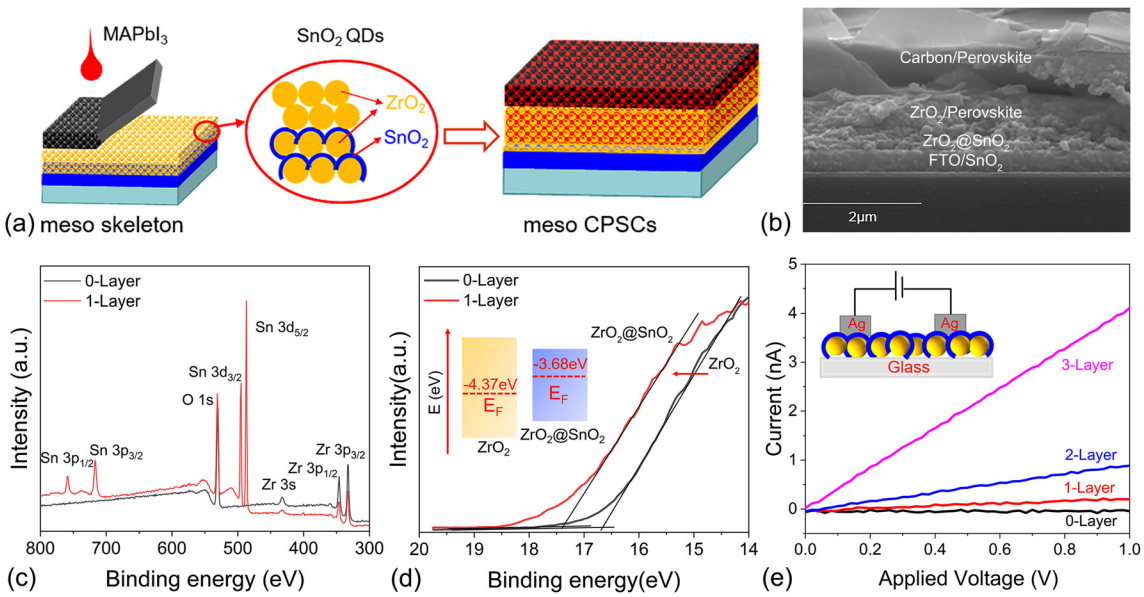

FIG. 1. (a) Schematic of the preparation process of low-temperature, mesoscopic CPSCs using SnO_2 modified meso-ZrO_2 as the electron-transport layer. (b) Cross-sectional SEM image of meso CPSC after filling of perovskite. (c) X-ray photoelectron spectroscopy of meso-ZrO_2 and meso-ZrO_2@SnO_2 thin layers. (d) Ultraviolet photoelectron spectroscopy of ZrO_2 and ZrO_2@SnO_2. (e) Current–voltage curve of meso-ZrO_2 modified by different layers of SnO_2.

4.37 eV could be recorded for ZrO_2. After the SnO_2 modification, it shifts upward to 3.68 eV. Such shift could be well-understood, since SnO_2 is known to be a N-type semiconductor. To better illustrate the electrical properties, the conductivity of the SnO_2 modified meso-ZrO_2 is measured by current–voltage scanning using architecture shown in Fig. 1(e). Clearly, the conductivity of meso-ZrO_2 increases after the modification of SnO_2.

The effect of the SnO_2 modification on the charge extraction properties is studied. Photoluminescence (PL) mapping is performed on devices by monitoring the spatial distribution of luminescence wavelength of 765 nm (according to CH_3NH_3I, or MA based perovskite).[34] From Fig. 2(a), one can see that before the SnO_2 modification on ZrO_2, PL signal with intensity higher than 10 000 (upmost to 17 500) is seen on the most part of the tested area. After one-layer SnO_2 is coated, the PL intensity is weakened by ~70%, with the upmost intensity lowering down to 5500. A similar distribution is observed when more layers of SnO_2 are coated. According to the XRD studies, crystallization behavior of perovskite is not affected by the modification layers, and, thus, the lowered PL intensity is ascribed to the improved charge extraction behavior across the interface between perovskite and meso ETL.[35–37] For comparison, time-resolved photoluminescence (TRPL) spectra are recorded on half-devices, where the top carbon electrode is peeled off. Typical TRPL curves are shown in Fig. S3(d), the fitted lifetime (τ) is collected in Table S1. The averaged τ is 68.30, 17.38, 17.65, and 17.95 ns for the modification at 0, 1, 2, and 3 layers, respectively. The reduced lifetime is also ascribed to the accelerated charge extraction, coinciding well with the PL mapping test.[38,39]

Charge-extraction and recombination dynamics of the meso CPSCs device are further studied by transient photocurrent/photovoltage (TPC/TPV) decay curves, and impedance spectroscopy (IS), typical TPC/TPV curves, and the Nyquist plots are seen in Fig. S3. Charge transition time (t_d) and lifetime (τ_{cell}) of photo-generated charge carriers, series resistance (R_s), and interfacial charge transfer resistance (R_{ct}) are reduced from TPC/TPV curves and Nyquist plots and collected in Figs. 2(e)–2(h), respectively. When ZrO_2 is not modified, the transition time (t_d) is 3.24 (±0.37) μs, and after modified by one layer SnO_2, it decreases to 2.79 (±0.22) μs, though it increases slightly to 2.89 (±0.15) and 3.13(±0.31) μs for the two and three layer modification, respectively. On the contrary, the lifetime (τ_{cell}) is 4.96 (±0.85) μs before modification; after one-layer SnO_2 modification, it increases to 7.38(±0.56) μs, though it drops little after more layer modifications. As such, charge-extraction is accelerated, while recombination is retarded. The accelerated extraction could also be reflected by the evolvement of series resistance (R_s) and charge-transfer resistance (R_{ct}). As for R_s, it is 50.94 (±6.08) Ω before modification while decreasing to 35.62 (±3.04) Ω after one-layer modification. As for R_{ct}, it is 139.92 (±20.67) Ω before modification while dropping to 124.97 (±10.03) Ω after one-layer modification. These results show that SnO_2 modified mesoporous ZrO_2 (or meso-ZrO_2 @ SnO_2) can serve as efficient ETL. After SnO_2 modification, the contact between perovskite crystallites and ETL is strengthened, which benefits the charge-extraction and recombination processes. It is noted that ion migration might also affect the measurement. It is well-known that ion migration is caused by defects and electrical stress in the device. Due to ion migration behavior, ion accumulation could happen, and then which leads to more defects and higher capacitance[40] affects aforementioned tests. However, as to ion migration itself, it usually happens in time-scale of seconds according to previous studies,[41,42] which is much slower than the charge-extraction and recombination processes. Accordingly, ion migration itself might bring less effect to these tests. On the contrary, lifetime (τ_{cell}) derived from TPV reflects the recombination of photogenerated charge carriers in full device.[43–45] It differs

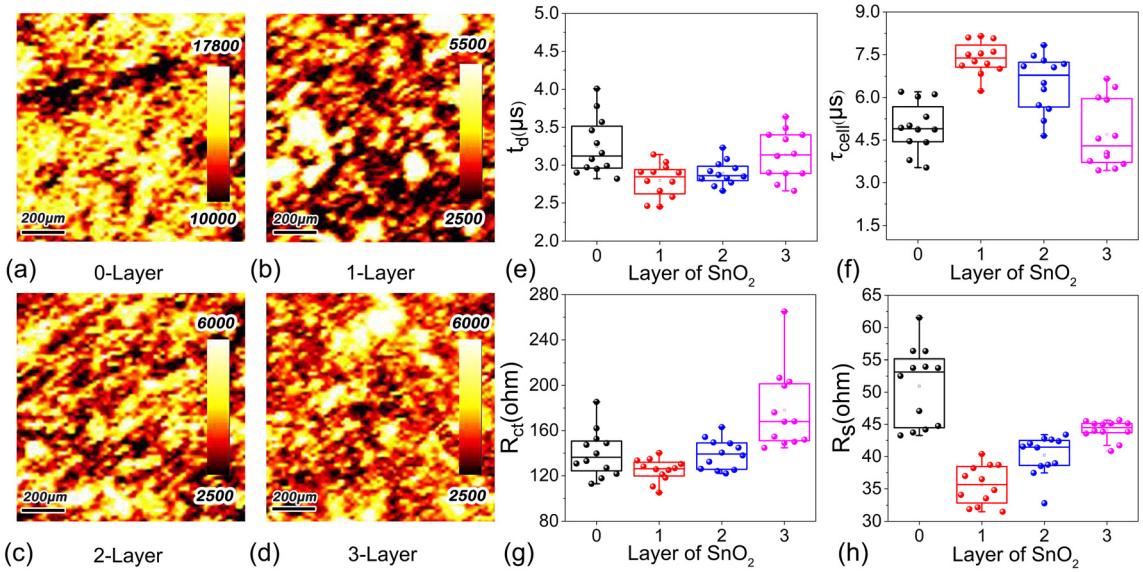

FIG. 2. (a)–(d) Photoluminescence (PL) mapping of meso CPSCs using SnO_2 modified mesoporous ZrO_2 (noted by meso-ZrO_2 @ SnO_2) as ETL (all mappings were taken from the substrate side). The effect of the SnO_2 modification layer on (e) transition time (t_d) and (f) lifetime (τ_{cell}) of photogenerated charge carrier in the low-temperature devices. The effect of the modification layer of SnO_2 on (g) charge transfer resistance (R_{ct}) and (h) series resistance (R_s) of the low-temperature mesoscopic perovskite solar cells based on carbon electrode.

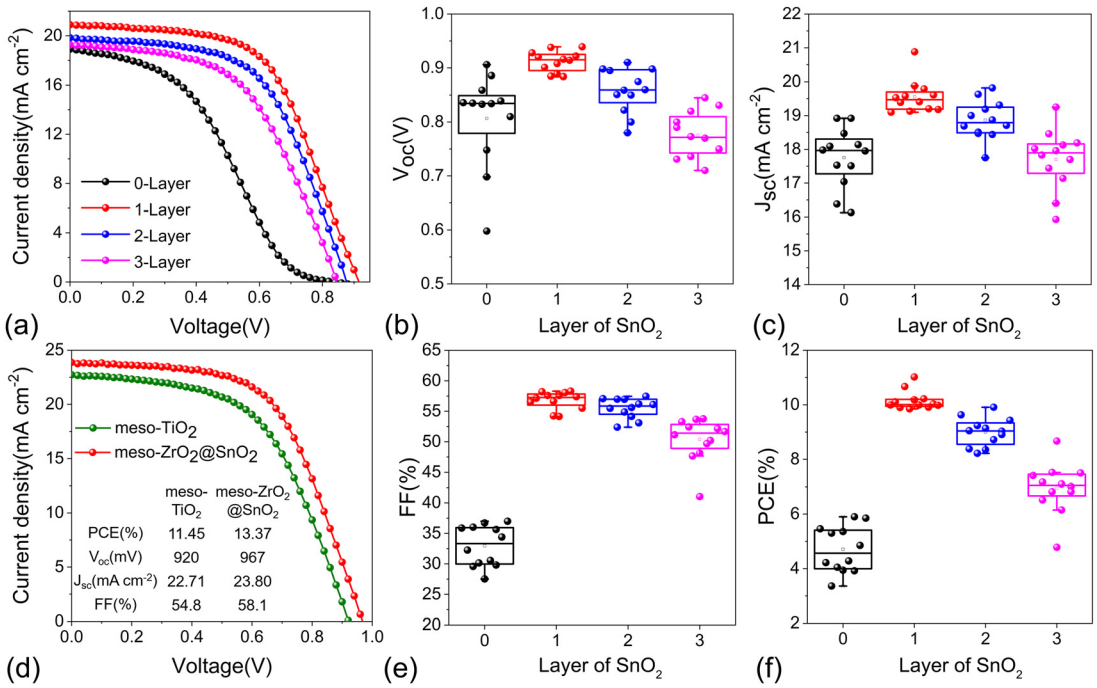

FIG. 3. (a) Effect of the modification layer of SnO_2 on current-density voltage characteristics of low-temperature meso CPSCs (AM 1.5 G, 100 mW cm^{-2}, test area is 0.0514 cm^2, recorded by reverse scan). Statistics on performance parameters (reverse scans): (b) V_{oc}, (c) J_{sc}, (e) FF, and (f) PCE. (d) Typical current–density voltage (J–V) curves of devices using TiO_2 or meso ZrO_2@SnO_2 as meso ETL.

from the "lifetime (τ)" measured from TRPL. However, when the charge-transport layer is used, lifetime (τ) could also be affected by the interfacial charge-extraction process. Smaller τ usually implies quicker extraction process, given that similar perovskite is monitored.[32,46,47] The accelerated charge-extraction and reduced charge recombination are beneficial for the power conversion processes. Typical current density–voltage (JV) curves are shown in Fig. 3(a). When there is no meso ETL, the "S-shape" JV curve appears, showing that the charge extraction process is highly retarded. In fact, ZrO_2 is a kind of insulator that could not serve as ETL. The observed JV curve is due to the possible contact between PVSK and the compact SnO_2 ETL, since the ZrO_2 layer is mesoporous. Then, after the bottom layer of ZrO_2 is modified by SnO_2, meso ETL is provided, and normal JV curves appear, indicating that the fluent extraction process happens. For a detailed comparison, all of the four performance parameters are collected and shown in Figs. 3(b), 3(c), 3(e), and 3(f) and Table S2, including open-circuit voltage (V_{oc}), short-circuit current density (J_{sc}), fill factor (FF), and power conversion efficiency (PCE). One can see that SnO_2 modification could upgrade all of the four parameters, while one-layer modification comes out with the optimized performance. Typically, after one-layer SnO_2 modification, V_{oc} increases from 806 (±86) to 912 (±19) mV, J_{sc} increases from 17.75 (±0.89) to 19.55 (±0.48) mA cm^{-2}, FF rises from 32.95 (±3.34)% to 56.78 (±1.44)%, and PCE upgrades from 4.70 (±0.85)% to 10.15 (±0.35)% [statistical histogram on *PCE* is shown in Fig. S4(a)]. In addition, examination of Figs. 2 and 3 shows that when charge extraction is accelerated (seeing lower t_d and lower R_{ct}), higher J_{sc} is harvested; when recombination is retarded (seeing increased τ_{cell}), higher V_{oc} is the resultant. Such phenomenon is, indeed, similar to that observed before,[48–50] depicting close relation between these parameters. It is worthy to note that as the modification layer increases, slight decline is seen in performance parameters. One possible reason rises from the fact of that more modification layers make the thicker SnO_2 layer, which reduces the porosity of the ETL, and the contact between perovskite and the ETL. However, more studies are needed in the future.

The performance of the low-temperature meso CPSCs based on meso-ZrO_2@SnO_2 is comparable to that based on meso-TiO_2. Typical JV curves are shown in Fig. 3(d), while corresponding performance parameters and PCE histogram are shown in Figs. S4(b) and S5. Meso-ZrO_2 @ SnO_2 based devices come out with slightly higher PCEs, with the optimized value of 13.37% (reverse scan) compared to

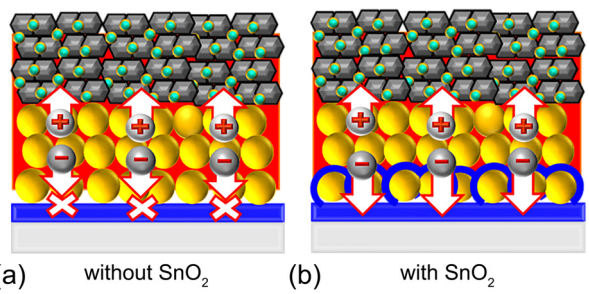

FIG. 4. (a) and (b) Schematics showing the effect of SnO_2 modification on the contact and electron-extraction process between the interface of perovskite crystallite and ETL.

11.45% of meso-TiO_2 devices. From Fig. S5, one can see that the main contribution is from V_{oc}. TPV study (shown in Fig. S6) observes longer lifetime in the case of meso-ZrO_2 @ SnO_2. Thus, lower recombination is reduced. The reduced recombination might arise from difference between the TiO_2 and SnO_2. Usually, it is suggested that SnO_2 owns lower conduction band bottom than TiO_2.[29,51] Accordingly, one may expect higher V_{oc} in meso TiO_2 devices, which differs from current study. As a result, other causes should be considered. It is well-known that, to obtain high crystallinity in TiO_2 nanoparticles, high temperature annealing (~450 °C) is usually needed. Without such high temperature treatment, there exists risk of presence relative higher surface defects. In contrast, low-temperature processed SnO_2 has helped to obtain high V_{oc} near 1000 mV in low temperature planar CPSCs,[17] and V_{oc} even higher than 1200 mV in metal-electrode based PSCs. Therefore, the reduced recombination might arise from the reduced surface defect.

To explain the observations relating to SnO_2 modification, schematics are shown in Figs. 4(a) and 4(b). When there is no meso ETL, incomplete contact is obtained between perovskite crystallites and ETL, leading to hindered electron-extraction. After the bottom ZrO_2 layer is modified with SnO_2, the contact is strengthened, ensuring effective electron-extraction and power conversion processes. Storage-stability is also tracked by storing the device in open air (relative humidity of 40%–50%, without encapsulation). As shown in Fig. S7, after 3000-h storage in the open air, no apparent decline is seen in efficiency. Moreover, slight increase is observed in the first few day storage, which relates to the slow coarsening process of perovskite grains in the mesoporous framework.[17]

Honestly, performance parameters of the currently studied low-temperature processed meso CPSCs are relatively lower than counter devices prepared by high temperature procedures.[19] The main problem lies on the lower V_{oc} and FF. In addition, hysteresis is observed (shown in Fig. S8), which is caused by defects.[40] These problems are relating to the relatively poor crystallinity of perovskite in the confined structure, and, thus, more studies are needed.

In summary, SnO_2 modified meso ZrO_2 is used to be a kind of mesoporous ETL for the low-temperature mesoscopic PSCs based on carbon electrode. With the combination of PL mapping, TRPL, TPC/TPV, and IS studies, it is shown that SnO_2 modification could accelerate electron-extraction while retard recombination, which helps to obtain a conversion efficiency of 13.37% (reverse scan) (AM1.5G, 100 mW cm^{-2}) and storage-stability up to 3000 h for the low-temperature devices. As a result, SnO_2 modified meso ZrO_2 could serve as an efficient ETL.

See the supplementary material for the device preparation and characterization; cross-sectional SEM image and corresponding element distribution maps (EDS) (Fig. S1); x-ray diffraction patterns (Fig. S2); typical TPC/TPV decay curves; Nyquist plots and time-resolved PL (Fig. S3); statistic histogram on PCEs (Fig. S4); statistics of performance parameters (Fig. S5); TPV decay curves for devices based on meso-TiO_2 and meso-ZrO_2 @ SnO_2 (Fig. S6); storage-stability (Fig. S7); hysteresis index (Fig. S8); fitted time constant from TRPL (Table S1); and statistics on performance parameters (Table S2).

C.Z. acknowledges the financial support of the National Scientific Foundation of China (NSFC, No. 61774170) and Hunan Provincial Natural Science Foundation (No. 2020JJ4759). Y.G. acknowledges support from the National Science Foundation, United States (NSF, No. DMR-1903962).

AUTHOR DECLARATIONS

Conflict of Interest

The authors have no conflicts to disclose.

Author Contributions

De'en Guo: Investigation (lead); Methodology (lead); Writing – original draft (lead). **Jiao Ma:** Methodology (supporting). **Siyuan Lin:** Methodology (supporting). **Xiao Guo:** Formal analysis (supporting). **Han Huang:** Formal analysis (equal). **Deming Kong:** Formal analysis (supporting); Investigation (supporting); Visualization (supporting). **Fuxin Xu:** Formal analysis (supporting). **Yongli Gao:** Formal analysis (supporting). **Wenhao Zhang:** Formal analysis (supporting). **Yue Hu:** Formal analysis (supporting). **Conghua Zhou:** Conceptualization (equal); Data curation (equal); Formal analysis (equal); Investigation (equal); Methodology (equal); Writing – original draft (equal).

DATA AVAILABILITY

The data that support the findings of this study are available within the article and its supplementary material.

REFERENCES

[1]A. Kojima, K. Teshima, Y. Shirai, and T. Miyasaka, J. Am. Chem. Soc. **131**(17), 6050 (2009).
[2]C. Zuo, H. J. Bolink, H. Han, J. Huang, D. Cahen, and L. Ding, Adv. Sci. **3**(7), 1500324 (2016).
[3]H. Min, D. Y. Lee, J. Kim, G. Kim, K. S. Lee, J. Kim, M. J. Paik, Y. K. Kim, K. S. Kim, and M. G. Kim, Nature **598**(7881), 444 (2021).
[4]See https://www.nrel.gov/pv/cell-efficiency.html for information about the best research-cell efficiency chart.
[5]Q. Chen, L. Chen, F. Y. Ye, T. Zhao, F. Tang, A. Rajagopal, Z. Jiang, S. L. Jiang, A. K. Y. Jen, Y. Xie, J. H. Cai, and L. W. Chen, Nano Lett. **17**(5), 3231 (2017).
[6]S. Liu, Y. Guan, Y. Sheng, Y. Hu, Y. Rong, A. Mei, and H. Han, Adv. Energy Mater. **10**(13), 1902492 (2020).
[7]Q. Jiang, X. Zhang, and J. You, Small **14**(31), 1801154 (2018).
[8]L. Meng, J. You, T.-F. Guo, and Y. Yang, Acc. Chem. Res. **49**(1), 155 (2016).
[9]Y. Rong, X. Hou, Y. Hu, A. Mei, L. Liu, P. Wang, and H. Han, Nat. Commun. **8**(1), 14555 (2017).
[10]Y. Xiong, X. Zhu, A. Mei, F. Qin, S. Liu, S. Zhang, Y. Jiang, Y. Zhou, and H. Han, Sol. RRL **2**(5), 1800002 (2018).
[11]J. Du, S. Liu, J. Wu, W. Zhang, W. Zhang, A. Mei, Y. Rong, Y. Hu, and H. Han, Sol. RRL **4**(12), 2000455 (2020).
[12]X. Chen, Y. Xia, Q. Huang, Z. Li, A. Mei, Y. Hu, T. Wang, R. Cheacharoen, Y. Rong, and H. Han, Adv. Energy Mater. **11**(18), 2100292 (2021).
[13]Z. Wei, K. Yan, H. Chen, Y. Yi, T. Zhang, X. Long, J. Li, L. Zhang, J. Wang, and S. Yang, Energy Environ. Sci. **7**(10), 3326 (2014).
[14]K. Yan, Z. Wei, J. Li, H. Chen, Y. Yi, X. Zheng, X. Long, Z. Wang, J. Wang, and J. Xu, Small **11**(19), 2269 (2015).
[15]Z. Yu, B. Chen, P. Liu, C. Wang, C. Bu, N. Cheng, S. Bai, Y. Yan, and X. Zhao, Adv. Funct. Mater. **26**(27), 4866 (2016).
[16]X. Meng, J. Zhou, J. Hou, X. Tao, S. H. Cheung, S. K. So, and S. Yang, Adv. Mater. **30**(21), 1706975 (2018).
[17]J. Yan, S. Lin, X. Qiu, H. Chen, K. Li, Y. Yuan, M. Long, B. Yang, Y. Gao, and C. Zhou, Appl. Phys. Lett. **114**(10), 103503 (2019).
[18]X. Xiao, Y. Chu, C. Zhang, Z. Zhang, Z. Qiu, C. Qiu, H. Wang, A. Mei, Y. Rong, G. Xu, Y. Hu, and H. Han, Fundam. Res. **1**(4), 385 (2021).
[19]S. Liu, D. Zhang, Y. Sheng, W. Zhang, Z. Qin, M. Qin, S. Li, Y. Wang, C. Gao, Q. Wang, Y. Ming, C. Liu, K. Yang, Q. Huang, J. Qi, Q. Gao, K. Chen, Y. Hu, Y. Rong, X. Lu, A. Mei, and H. Han, Fundam. Res. **2**(2), 276 (2022).

[20]Y. Yang, Z. Liu, W. K. Ng, L. Zhang, H. Zhang, X. Meng, Y. Bai, S. Xiao, T. Zhang, and C. Hu, Adv. Funct. Mater. **29**(1), 1806506 (2019).
[21]T. Tian, J.-X. Zhong, M. Yang, W. Feng, C. Zhang, W. Zhang, Y. Abdi, L. Wang, B.-X. Lei, and W.-Q. Wu, Angew. Chem. Int. Ed. **60**(44), 23735 (2021).
[22]A. Y. Mei, Y. S. Sheng, Y. Ming, Y. Hu, Y. G. Rong, W. H. Zhang, S. L. Luo, G. R. Na, C. B. Tian, X. M. Hou, Y. L. Xiong, Z. H. Zhang, S. Liu, S. Uchida, T. W. Kim, Y. B. Yuan, L. J. Zhang, Y. H. Zhou, and H. W. Han, Joule **4**(12), 2646 (2020).
[23]C. Zhou and S. Lin, Sol. RRL **4**(2), 1900190 (2020).
[24]H. Zhou, Y. Shi, K. Wang, Q. Dong, X. Bai, Y. Xing, Y. Du, and T. Ma, J. Phys. Chem. C **119**(9), 4600 (2015).
[25]Z. Wei, H. Chen, K. Yan, and S. Yang, Angew. Chem. Int. Ed. **53**(48), 13239 (2014).
[26]H. Zhang, Y. Li, S. Tan, Z. Chen, K. Song, S. Huang, J. Shi, Y. Luo, D. Li, and Q. Meng, J. Colloid Interface Sci. **608**(3), 3151 (2022).
[27]S. N. Vijayaraghavan, J. Wall, L. Li, G. Xing, Q. Zhang, and F. Yan, Mater. Today Phys. **13**, 100204 (2020).
[28]T. Shi, S. Lin, M. Fang, D. Kong, Y. Yuan, Y. Gao, B. Yang, H. Han, and C. Zhou, Appl. Phys. Lett. **117**(16), 163501 (2020).
[29]G. Yang, C. Chen, F. Yao, Z. Chen, Q. Zhang, X. Zheng, J. Ma, H. Lei, P. Qin, L. Xiong, W. Ke, G. Li, Y. Yan, and G. Fang, Adv. Mater. **30**(14), 1706023 (2018).
[30]L. Xiong, Y. Guo, J. Wen, H. Liu, G. Yang, P. Qin, and G. Fang, Adv. Funct. Mater. **28**(35), 1802757 (2018).
[31]W. Ke, G. Fang, Q. Liu, L. Xiong, P. Qin, H. Tao, J. Wang, H. Lei, B. Li, J. Wan, G. Yang, and Y. Yan, J. Am. Chem. Soc. **137**(21), 6730 (2015).
[32]J. P. C. Baena, L. Steier, W. Tress, M. Saliba, S. Neutzner, T. Matsui, F. Giordano, T. J. Jacobsson, A. R. S. Kandada, S. M. Zakeeruddin, A. Petrozza, A. Abate, M. K. Nazeeruddin, M. Gratzel, and A. Hagfeldt, Energy Environ. Sci. **8**(10), 2928 (2015).
[33]G. Liu, B. Yang, B. Liu, C. Zhang, S. Xiao, Y. Yuan, H. Xie, D. Niu, J. Yang, Y. Gao, and C. Zhou, Appl. Phys. Lett. **111**(15), 153501 (2017).
[34]Z. Shao, J. Xiao, X. Guo, S. You, Y. Zhang, M. Li, F. Song, C. Zhou, H. Xie, Y. Gao, J. Sun, and H. Huang, Curr. Appl. Phys. **36**, 27 (2022).
[35]J. Wei, F. Guo, X. Wang, K. Xu, M. Lei, Y. Liang, Y. Zhao, and D. Xu, Adv. Mater. **30**(52), 1805153 (2018).
[36]K. Deng, Q. Chen, and L. Li, Adv. Funct. Mater. **30**(46), 2004209 (2020).
[37]P. Zhu, S. Gu, X. Luo, Y. Gao, S. Li, J. Zhu, and H. Tan, Adv. Energy Mater. **10**(3), 1903083 (2020).
[38]Q. Jiang, L. Zhang, H. Wang, X. Yang, J. Meng, H. Liu, Z. Yin, J. Wu, X. Zhang, and J. You, Nat. Energy **2**(1), 16177 (2017).
[39]D. Yang, R. Yang, K. Wang, C. Wu, X. Zhu, J. Feng, X. Ren, G. Fang, S. Priya, and S. Liu, Nat. Commun. **9**, 3239 (2018).
[40]Y. Yuan and J. Huang, Acc. Chem. Res. **49**(2), 286 (2016).
[41]J. Xing, Q. Wang, Q. Dong, Y. Yuan, Y. Fanga, and J. Huang, Phys. Chem. Chem. Phys. **18**(44), 30484 (2016).
[42]J. Zhang, C. Li, M. Chen, and K. Huang, J. Phys. D: Appl. Phys. **54**(4), 044002 (2021).
[43]Y. Shao, Y. Yuan, and J. Huang, Nat. Energy **1**, 15001 (2016).
[44]B. Chen, Z. Yu, K. Liu, X. Zheng, Y. Liu, J. Shi, D. Spronk, P. N. Rudd, Z. Holman, and J. Huang, Joule **3**(1), 177 (2019).
[45]Y. Chen, N. Li, L. Wang, L. Li, Z. Xu, H. Jiao, P. Liu, C. Zhu, H. Zai, M. Sun, W. Zou, S. Zhang, G. Xing, X. Liu, J. Wang, D. Li, B. Huang, Q. Chen, and H. Zhou, Nat. Commun. **10**, 1112 (2019).
[46]Q. Cao, Y. Li, H. Zhang, J. Yang, J. Han, T. Xu, S. Wang, Z. Wang, B. Gao, J. Zhao, X. Li, X. Ma, S. M. Zakeeruddin, W. E. I. Sha, X. Li, and M. Graetzel, Sci. Adv. **7**(28), eabg0633 (2021).
[47]Y. Hu, Z. Zhang, A. Mei, Y. Jiang, X. Hou, Q. Wang, K. Du, Y. Rong, Y. Zhou, G. Xu, and H. Han, Adv. Mater. **30**(11), 1705786 (2018).
[48]H. Chen, K. Li, H. Liu, Y. Gao, Y. Yuan, B. Yang, and C. Zhou, Org. Electron. **61**, 119 (2018).
[49]G. Liu, B. Yang, H. Chen, Y. Zhao, H. Xie, Y. Yuan, Y. Gao, and C. Zhou, Appl. Phys. Lett. **115**(21), 213501 (2019).
[50]Q.-Q. Chu, B. Ding, J. Peng, H. Shen, X. Li, Y. Liu, C.-X. Li, C.-J. Li, G.-J. Yang, and T. P. White, J. Mater. Sci. Technol. **35**(6), 987 (2019).
[51]A. Mei, X. Li, L. Liu, Z. Ku, T. Liu, Y. Rong, M. Xu, M. Hu, J. Chen, and Y. Yang, Science **345**(6194), 295 (2014).